Elsevier Editorial System(tm) for
Microporous & Mesoporous Materials
Manuscript Draft

Manuscript Number: MICMAT-D-18-01176R2

Title: Probing the confinement of β-galactosidase into meso-macro porous silica by Raman spectroscopy

Article Type: Full length article

Keywords: β-galactosidase, biocatalysts, meso-macroporous silica, enzyme-support interactions, Raman spectroscopy.

Corresponding Author: Dr. Gemma Montalvo, Ph.D.

Corresponding Author's Institution: University of Alcalá

First Author: Sofia F Prazeres, Master

Order of Authors: Sofia F Prazeres, Master; Félix Zapata, Master; Nadia Canilho, PhD; Andreea Pasc, PhD; Carmen García-Ruiz, PhD; Gemma Montalvo, Ph.D.

Abstract: Immobilization of β-galactosidase (β-gal) into porous materials might afford to supported biocatalysts for the hydrolysis of diary products or to food additives for lactose intolerant people. Activity and stability of the loaded material generally depend on the interactions between the enzyme and the support, as well as on the pore size. Herein, Raman spectroscopy was used to evaluate the specific adsorption the enzyme into meso-macroporous silica materials, containing interconnected mesopores of 9 nm and macropores of 200 nm. Non-porous silica was used as reference material to determine the Raman fingerprint of physisorbed enzyme in the absence of any confinement. While the β-gal physisorbed on the surface of non-porous silica material exhibits the same Raman spectra as the free enzyme, the enzyme physisorbed onto meso-macroporous materials show frequency displacements of characteristic amide groups as a function of initial concentration of the feed enzymatic solution. In fact, at low initial concentration in enzyme, no shifts of the amides were recorded on Raman spectra as compared with free enzyme, indicating a preferential physisorption into macropores. By increasing the enzyme concentration, the frequency of Amide I was shifted to lower values, suggesting thus a confinement into mesopores. Finally, the enzyme concentration effect can be demonstrated by the increment of the amide band intensity in the range of 1700-1500 cm-1 as the amount of adsorbed enzyme increases. Thus, the textural properties of silica materials seem to be the key factor in the enzyme adsorption.

HIGHLIGHTS

1. β-gal physisorbed on the surface of non-porous silica material or into macropores exhibits the same Raman fingerprint as the free enzyme
2. The characteristic amide bands of β-gal physisorbed into mesopores are red shifted compared to free enzyme
3. Spectral Raman fingerprint probes the confinement of β-galactosidase into meso-macro porous silica.

Probing the confinement of *β*-galactosidase into meso-macro porous silica by Raman spectroscopy

Sofia F. Prazeres[1], Félix Zapata[1,2], Nadia Canilho[3], Andreea Pasc[3], Carmen García-Ruiz[1, 2]; Gemma Montalvo[1, 2,*]

[1]Department of Analytical Chemistry, Physical Chemistry and Chemical Engineering, University of Alcalá, Ctra. Madrid-Barcelona Km. 33.600, 28871 Alcalá de Henares, Madrid, Spain

[2]University Institute of Research in Police Sciences, University of Alcalá, Ctra. Madrid-Barcelona Km. 33.600, 28871 Alcalá de Henares, Madrid, Spain

[3]L2CM UMR 7053 CNRS-Universite de Lorraine, Bvd des Aiguillettes, BP 70239, F-54506 Vandoeuvre-les-Nancy, France

* Corresponding author: gemma.montalvo@uah.es

*Graphical Abstract

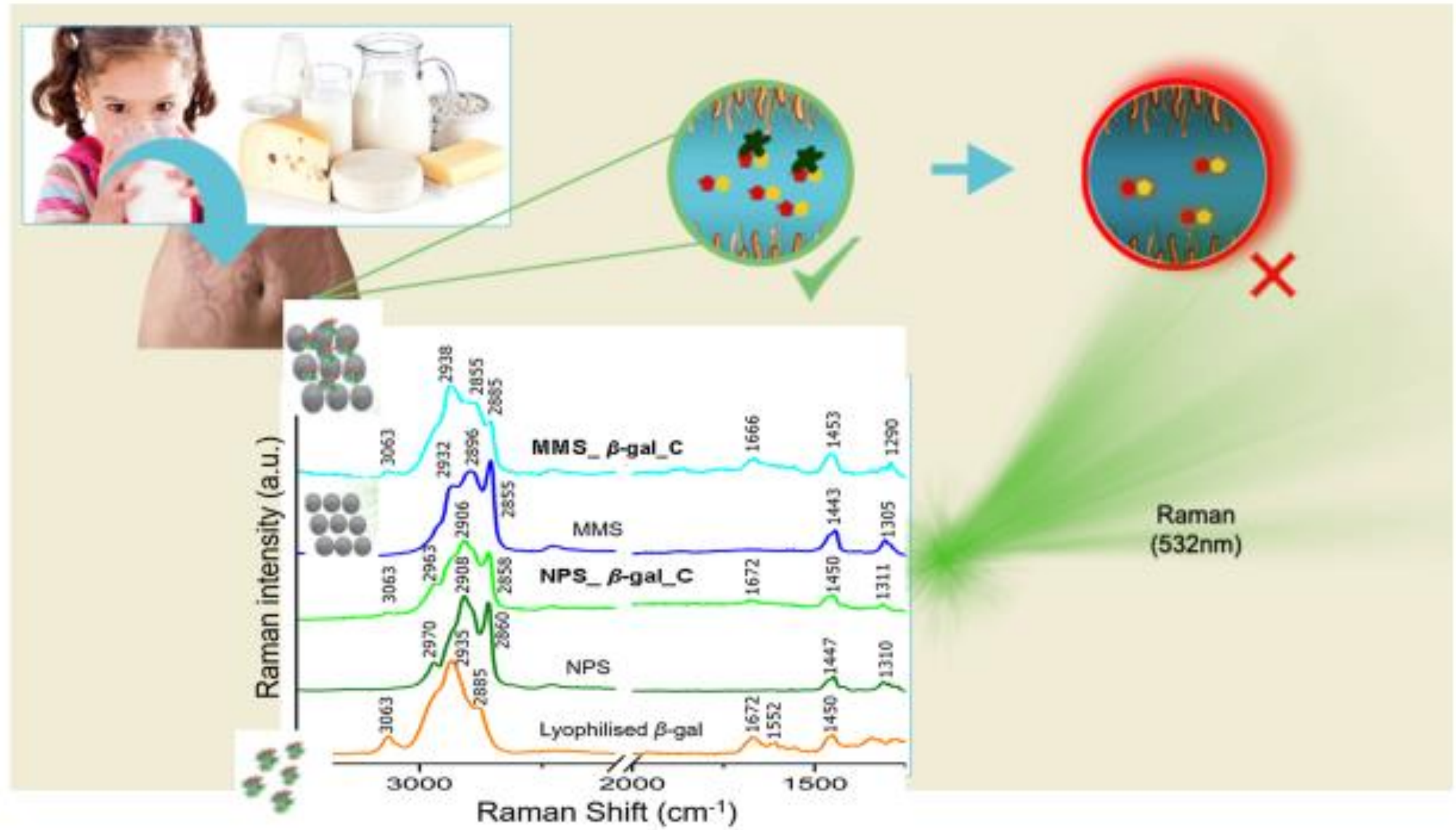

Probing the confinement of *β*-galactosidase into meso-macro porous silica by Raman spectroscopy

Sofia F. Prazeres[1], Félix Zapata[1,2], Nadia Canilho[3], Andreea Pasc[3], Carmen García-Ruiz[1, 2]; Gemma Montalvo[1, 2,*]

[1]Department of Analytical Chemistry, Physical Chemistry and Chemical Engineering, University of Alcalá, Ctra. Madrid-Barcelona Km. 33.600, 28871 Alcalá de Henares, Madrid, Spain

[2]University Institute of Research in Police Sciences, University of Alcalá, Ctra. Madrid-Barcelona Km. 33.600, 28871 Alcalá de Henares, Madrid, Spain

[3]L2CM UMR 7053 CNRS-Universite de Lorraine, Bvd des Aiguillettes, BP 70239, F-54506 Vandoeuvre-les-Nancy, France

* Corresponding author: gemma.montalvo@uah.es

Highlights

1. *β*-gal physisorbed on the surface of non-porous silica material or into macropores exhibits the same Raman fingerprint as the free enzyme.
2. The characteristic amide bands of *β*-gal physisorbed into mesopores are red shifted compared to free enzyme.
3. Spectral Raman fingerprint probes the confinement of *β*-galactosidase into meso-macro porous silica.

Abstract

Immobilization of *β*–galactosidase (*β*-gal) into porous materials might afford to supported biocatalysts for the hydrolysis of diary products or to food additives for lactose intolerant people. Activity and stability of the loaded material generally depend on the interactions between the enzyme and the support, as well as on the pore size. Herein, Raman spectroscopy was used to evaluate the specific adsorption the enzyme into meso-macroporous silica materials, containing interconnected mesopores of 9 nm and macropores of 200 nm. Non-porous silica was used as reference material to determine the Raman fingerprint of physisorbed enzyme in the absence of any confinement. While the *β*-gal physisorbed on the surface of non-porous silica material exhibits the same Raman spectra as the free enzyme, the enzyme physisorbed onto meso-macroporous materials show frequency displacements of characteristic amide groups as a function of initial concentration of the feed enzymatic solution. In fact, at low initial concentration in enzyme, no shifts of the amides were recorded on Raman spectra as compared with free enzyme, indicating a preferential physisorption into macropores. By increasing the enzyme concentration, the frequency of Amide I was shifted to lower values, suggesting thus a confinement into mesopores. Finally, the enzyme concentration effect can be demonstrated by the increment of the amide band intensity in the range of 1700-1500 cm^{-1} as the amount of adsorbed enzyme increases. Thus, the textural properties of silica materials seem to be the key factor in the enzyme adsorption.

Keywords: *β*-galactosidase, biocatalysts, meso-macroporous silica, enzyme-support interactions, Raman spectroscopy.

1. Introduction

Immobilization of biomolecules (i.e. proteins, DNA) into nanostructured materials is extensive area of research. This is particularly relevant for designing sustainable biocatalysts and biosensors, allowing for multiple reuses and for the protection of biomolecules from denaturating external factors or operational parameters such as temperature, pH or reactive species [1-5]. Many organic or inorganic porous supports such as polymers, carbon nanotubes or particles, metal-oxides, glass or porous silica materials have been investigated for biomolecules immobilization, especially due to their capacity of loading as well as mechanical and chemical stability [4]. Among those supports, ordered porous silica materials are the most widely chosen for the following main reasons: the tunability of the surface chemical functions and the control of the pore size to fit with the biomolecule diameter and to increase the specific surface of the support [6-9].

Enzyme-supported silica materials already found industrial and biotechnological applications, including in food industry. In this field, one challenge still lies in finding solutions for lactose intolerant consumers, such as for the production of low-lactose products. This could be achieved by using lactase enzymes, *e.g.* β-galactosidase (β-gal). The immobilization of β-gal into porous materials might afford to supported biocatalysts for the hydrolysis of dairy products or to food additives for lactose intolerant people. The enzyme immobilization on a support material is a good solution to protect the enzyme from external conditions as pH and temperature [10-11]. Among several materials (such chitosan, agarose, and cellulose) [12-13], the porous silica materials have been widely used as support materials for the immobilization of β-galactosidase [12-20], mainly due to their large interacting surface and the precise tuning of the pore sizes. Several strategies have been applied for controlled delivery of β-gal, using both physical and covalent immobilization of the enzyme. In brief, the attachment of a lactose derivative as gatekeeper on the surface of mesoporous silica nanoparticles has resulted in successful enzyme-responsive intracellular controlled delivery of biologically active enzyme β-gal into cells, which provides promising delivery systems for large therapeutic proteins [6, 7, 17]. Bernal et al. reported that the three-dimensional structure of the β-gal was not significantly affected during

79 the physical immobilization process on an hierarchical porous silica with a stable large porosity
80 (10-40 nm and 0.07-20 µm diameter ranges) [14]. Instead of that, *β*-gal presented a selective
81 physical adsorption on hierarchical meso-macroporous silica materials (average pore size 9 and
82 200 nm, respectively), arising from the oligomeric complexation of the enzyme (as
83 monomer/dimer/tetramer), which affected to the catalytic activity [18]. That enzyme had an
84 improvement of mechanical and thermal stability by multipoint covalent immobilization in
85 hierarchical macro-mesoporous silica (average mesoporous diameter 20 nm) [15].

86 The activity and stability of the loaded material generally depend on the interactions between
87 the enzyme and the support, as well as on the pore size. To gather further insights on those
88 specific interactions, vibrational spectroscopy (e.g. infrared and Raman spectroscopy) appear as
89 the most powerful as they provide information about molecular vibrations. Whereas IR spectra
90 depends on polar moment and tend to emphasize asymmetric vibrations of polar groups (*e.g.*
91 OH, C-H, N-H, C=O, etc.), Raman spectroscopy depends on polarizability changes and tends to
92 emphasize symmetric vibrations of non-polar groups such as C=C and C-C stretches, and
93 aromatic ring breathing vibrations [21]. Therefore, the frequencies of those molecular vibrations
94 depend not only on the atom masses and on their geometric arrangement, but also on the
95 strength of their chemical bonds and interactions. In addition, these techniques present several
96 attractive features such as being generally fast, non-destructive, and non-invasive.
97 Usually, the presence of enzymes on different supports has been demonstrated by the
98 appearance of amide bands in the IR spectrum [22-26]. However, only few of those studies are
99 addressing the fine interactions between the enzyme and the support that lead to different band
100 frequencies on the IR spectrum [22, 25]. Some authors have justified the interactions by the
101 frequency shift of the characteristics bands of the functional groups of the enzymes (mainly
102 amide) simply by an increase of the band intensity. In addition, different studies have also been
103 carried out by Raman spectroscopy for different enzymes/supports yielding information about
104 chemical modification occurring by functionalization, or the study of the enzyme structural
105 changes induced by the isotopically replacement of H_2O solvent by D_2O [27-31].

Indeed, very few studies on the physico-chemical interactions investigated by IR have dealt with the adsorption of *β*-gal on different support materials [18, 22, 24], whereas Raman spectroscopy has not yet been used specifically to identify and characterize *β*-gal immobilization. The goal of this work is to show the capabilities of Raman spectroscopy to characterize the specific adsorption of *β*-gal onto meso-macroporous silica substrates through the analysis of interactions between the enzyme and the silica support. It concerns more particularly the evaluation of the specific adsorption of the enzyme into meso-macroporous silica materials, containing interconnected mesopores of 9 nm and macropores of 200 nm. A non-porous silica material was used as reference to determine the Raman fingerprint of physisorbed enzyme in the absence of any confinement.

2. Experimental Sections

2.1. Materials

Two different silica supports were used: commercially available non-porous nanoparticles from Nanocomposites company (NPS, 97 nm diameter), and a porous, homemade material described by Pasc et al [32], which is a dual meso-macroporous silica (MMS). In brief, the synthesis protocol involved the preparation of a colloidal suspension of solid lipid nanoparticles of n-hexadecylpalmitate dispersed in a micellar solution of Pluronic P123 surfactant. A hybrid organo-silicate material was obtained by the hydrolysis and the polycondensation of tetramethoxysilane (TMOS) around to the colloidal template. The meso and macro porosities were released by Sohxlet extraction.

The *β*-gal enzyme solution, extracted from *Kluyveromyces lacti*s source, was a gift from Chr. Hansen Company (Copenhagen, Denmark). The stock solution provided is 80% pure enzyme (determined by SDS-PAGE analysis) and has a concentration of 40 mg/mL of protein in PEM buffer solution (phosphate, ethylenediaminetetraacetic acid (EDTA), and magnesium, pH 6.6) and glycerol (1:1) weight ratio. The enzyme activity of stock solution was measured at 5200 NLU/g. It was determined spectrophotometrically from its ability to convert *o*-nitrophenyl-*β*-D-

133 galactopyranoside (ONPG) into galactose and *o*-nitrophenol (ONP). Assay of *β*-gal activity was
134 described in reference [11]. One NLU is the quantity of enzyme that releases 1.3 μmol of o-
135 nitrophenol per min at 30°C and pH 6.5 [33]. All the buffer reagents were purchased from
136 Sigma-Aldrich (Spain).

137 ## 2.2. Immobilization of *β* –gal onto silica supports

138 The enzyme immobilization was performed on two types of silica supports (porous and non-
139 porous) through physical adsorption, by mixing the enzyme solution and the silica material in
140 the PEM buffer (pH 6.6), under agitation for 48 hours at room temperature. The amount of silica
141 was fixed (25 mg) and the *β*-gal concentration was varied according to the concentration of the
142 feed solution denoted as C/x, where x indicates the dilution factor. Thus, the C/x concentrations
143 ranged from C (40 mg/ml) to C/2, C/4, C/6, C/10 and C/20. After immobilization, samples were
144 washed 3 times with buffer solution, by centrifugation at 4000 rpm. Then, samples were dried at
145 room temperature, and a white powder was obtained. Finally, the samples were kept at room
146 temperature.

147 The protein loading in the respective silica materials were determined using a UVIKON 943
148 UV-Vis Kontron spectrophotometer, thought their absorption wavelength at 280 nm. To do so,
149 the absorbance of each supernatant recovered after the washing step was measured. Table 1
150 summarizes the amount of *β*-gal adsorbed on the MMS and was calculated as the difference
151 between the initial mount of protein in the respective adsorption solution and the residual
152 amount of the *β*-gal lost in the supernatant. The samples are denoted from now on as, for
153 example, "MMS_ *β*-gal_C/2" meaning dilution of factor 2 of the stock enzyme solution
154 adsorbed on the meso-macroporous silica support.

155 **Table 1.** Amount of *β*-gal adsorbed on MMS per surface area of MMS, for the different concentrations
156 of initial β-gal solutions used for immobilization.

Sample	Initial *β*-gal concentration (mg/mL)	Adsorbed *β*-gal (mg/ m^2)
MMS_*β*-gal_C	40	16
MMS_*β*-gal_C/2	20	10
MMS_*β*-gal_C/4	10	8.0
MMS_*β*-gal_C/6	6.7	6.9

MMS_β-gal_C/10	4.0	5.2
MMS_β-gal_C C/20	2.0	5.2

Concerning the sample NPS_ β-gal_C, the adsorbed enzyme was 0.117 mg/m^2 of silica NPS. That corresponds to two orders of magnitude lower than the analogous sample for the MMS support.

The immobilized enzyme was active for both silica systems and for all the different feed concentrations. As reported in previous work [18], the specific activity of the enzyme physisorbed in the macropores was two times higher (about 30-35 U/g) than that of the enzyme entrapped into mesopores (below 15 U/g), where 1 U corresponding to the amount of enzyme catalyzing the conversion of 1 μmol of ONPG per minute at 25 °C. For the NPS_ β-gal system, the activity was inspected qualitatively, verifying the yellow color after convert ONPG into galactose and ONP, when reaction was carried out by the same assay methodology than for the hierarchical porous silica system.

2.3. Characterization

2.3.1. Morphological properties

The morphology and the porosity at the bare silica materials were observed by Transmission (TEM) and Scanning (SEM) Electron Microscopy. The TEM pictures were carried out with a Philips CM200 at 200 kV and the Image processor software used was GATAN. The MMS powder was first ground and then suspended in ethanol (Sigma-Aldrich, France) by sonication. A drop of the dispersion was spread out on the TEM carbon lacey grid and dried at room temperature before observation. The SEM micrographs were obtained with a Zeiss DSM 950 scanning electron microscope using an acceleration voltage of 15kV. The NPS powder was lyophilized before to air-disperse on carbon grid followed by metal coating with a Polaron E-5400 equipment. The images were acquired from randomly chosen location and analysed with the scanning probe image processor software (Quartz PCI).

2.3.2. Structural properties

181 The elementary organic analysis of silica materials was performed using a LECO CHNS-932
182 Elementary Chemical Analyzer.
183 Fourier Transform Infrared spectroscopy (FTIR) measurements were performed using a Thermo
184 Scientific FT-IR Nicolet IS 10 (Waltham, MA, USA), equipped with an attenuated total
185 reflectance (ATR) sampling accessory with a diamond crystal. The version 6.0 of Omnic
186 software from Thermo Scientific was used for instrument control and spectra acquisition. Each
187 absorbance spectrum was recorded from 4000 to 400 cm^{-1} with a resolution of 4 cm^{-1} and the
188 signal averaged over 32 scans. The spectra of four independent spots of each sample were
189 collected, and then, a mean spectrum was calculated and finally normalized between 0 and 1.
190 Raman spectra were collected using a Thermo Scientific confocal DXR Raman Microscope
191 controlled by the Thermo Scientific OMNIC for dispersive Raman 8.3.103 software. A laser
192 emitting at 532 nm with 8 mW and a confocal slit size of 50 µm were used. The microscope was
193 set to 50x magnification under bright field illumination. Raman spectra of all samples were
194 collected in the range 3450-500 cm^{-1}. The spectral resolution of the used instrument ±2 cm^{-1}.
195 The number of scans was optimized for the different samples in order to obtain the best signal-
196 to-noise ratio (always within the range 5-50 scans), while the optimum exposure time for each
197 scan was fixed to 10 seconds. Fluorescence correction (polynomial order 6 of OMNIC
198 fluorescence correction) and smoothing (5 points, polynomial order 2) were applied. All Raman
199 spectra were finally normalized between 0 and 1 in order to facilitate the comparison between
200 the recorded spectra according the enzyme content and the silica support type.
201 No sample treatment was performed to bare silica materials, but the *β*-gal standard solution was
202 lyophilised before Raman analysis. Both silica supports were microscopically different.
203 Contrary to the homogeneous spherically shaped non-porous silica, the home synthetized meso-
204 macroporous silica showed a big heterogeneous surface. For both supports, focusing was an
205 extremely difficult task because the samples were composed of a white powder, assembled in
206 different layers inducing different surface depths. To avoid this problem, Raman spectra were
207 collected on a very small powder grain, but the laser spot size (about 1.2 µm) always resulted
208 smaller than the particle size. In addition, microscope glass slides were previously covered with

aluminium foil to avoid the spectral interferences caused by glass when measuring the particles of silica material.

Due to the heterogeneous adsorption (*i.e.* heterogeneous distribution of *β*-gal on silica supports), there were some spots, in particular for low enzyme contents, where the amide bands were intense and dominated the Raman spectra, and some other spots, where it was only possible to detect the bands of the silica material. To overcome this limitation, spectra from five random selected spots of the same sample were acquired at room temperature to record and averaged signal intensity.

The graphs presented in this paper have been plotted using the OriginPro® 9.1 software (Northampton, MA, USA).

3. Results and discussion

The *β*-gal was adsorbed in both types of silica materials as described in the experimental section. We proposed two different particles morphologies in order to inspect the capability of Raman spectroscopy to evaluate the strength of the expected different interaction between the enzyme and the two silica supports. The main difference between the systems is the confinement of the enzyme in the meso and macropores of the MMS materials.

Firstly, the morphology of the meso-macroporous silica and the non-porous silica was analysed by TEM and SEM, respectively, as shown in Figure 1. The non-porous silica are spherical particles of about 30 μm that display sporadically micro-craters of about 2 μm on the surface according to SEM photomicrographs (Fig. 1A). The MMS material support shows a dual meso-macroporosity of 9 nm and 100 nm, respectively (Fig. 1B). As determined from nitrogen sorption measurements [18], bare MMS material had a specific surface area of 660 m^2 g^{-1} and a pore volume of 1.23 cm^3 g^{-1}. The material exhibited a type IV isotherm, characteristic of a mesoporous material, with an average pore size of 9 nm, and a steep increase of the adsorbed volume at p/p_0 >0.9, confirming the presence of macropores. The *β*-gal is a homo-oligomer of four subunits with dimensions of 15.1 nm × 17.1 nm × 10.7 nm, as inferred from the crystal

structure, leading to an averaged hydrodynamic diameter of about 14 nm. On the other hand, the dimer and the monomer can be contained in boxes of dimensions 11.9 nm × 15.6 nm × 7.2 nm, and 7.2 nm × 11.7 nm × 6.3 nm, respectively. On the basis of this data, it was reasonably hypothesized that monomers and dimers can be adsorbed into the mesopores, while the tetramers can be physisorbed onto the macropores. As evidenced in previous work, the preference for being in dimer or tetramer form mainly depended on the enzyme concentration [18].

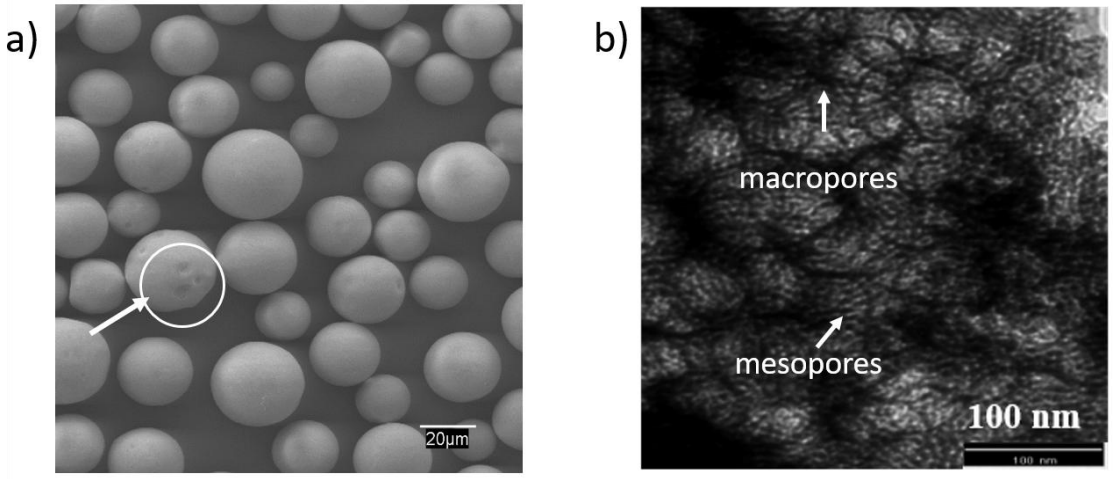

Figure 1. (A) SEM images of NPS particles where the arrows and the circles point the macropores and (B) TEM images of MMS.

The Raman spectra of both bare silica supports were recorded and compared with the signal of lyophilized free enzyme and loaded MMS and NPS silica materials at the highest concentration (MMS_ *β*-gal_C and NPS_ *β*-gal_C) as presented on Figure 2.

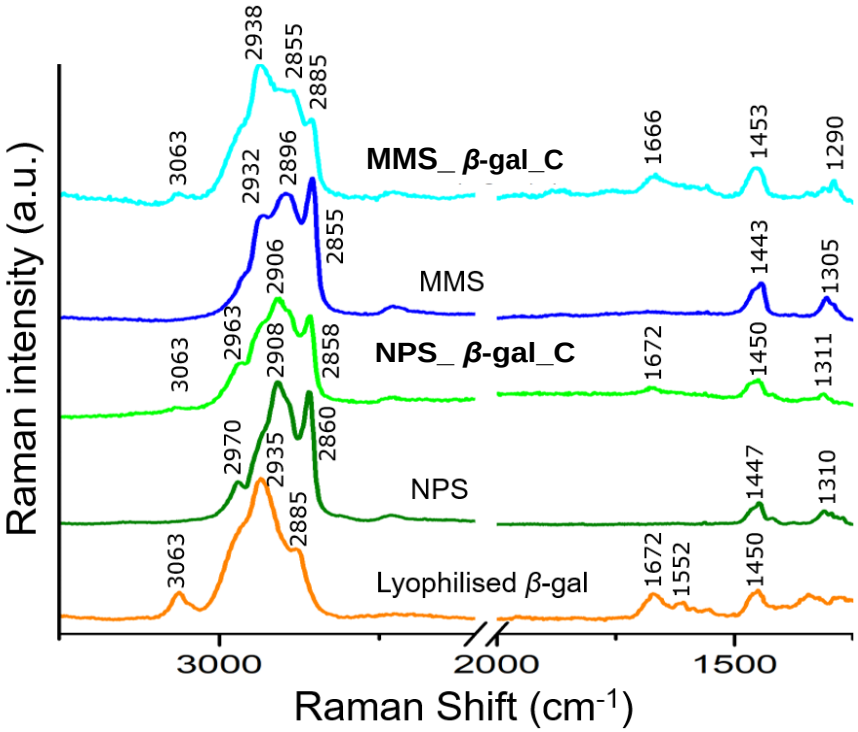

Figure 2: Raman spectra of NPS and MMS before and after *β*-gal immobilization (loaded at the maximum concentration, C, from the enzyme stock solutions). Raman spectra of lyophilized *β*-gal free enzyme is also provided for comparison purposes.

The spectra of both bare silica supports (MMS and NPS) present some bands in the range 3000-2500 cm^{-1}, which are assigned to the stretching vibrations of C-H groups. Particularly, they are related to the compounds used in the synthesis process of these silica materials, *i.e.* some traces of the surfactants and/or lipids used in the synthesis as templates can remain even after calcination [34]. This is in agreement with the thermogravimetric analysis of the MMS bare silica support that contains almost 21 wt % organics [18]. However, the Raman shift of the C-H bands of the non-porous silica material (2970, 2908, 2860 cm^{-1}), and the relative intensity of them, are different to the ones of the porous silica (2932, 2896, 2855 cm^{-1}). No information was available about the reagents used in the manufacture of the commercial non-porous silica support, but the elementary analyses support the presence of some organics too. The nitrogen and sulphur atoms are not present in the bare materials, which allows us to rule out the presence of bacterial contamination or microorganisms according to elemental analysis data.

Figure 2 also shows the spectrum of the lyophilised *β*-gal which exhibits a band at 3063 cm^{-1} due to N-H stretching vibrations, characteristic of amides and commonly designated as amide B band [28, 29]. There is also an overlap of several intense bands within the range 3000-2850 cm^{-1}

(maxima at 2935 cm^{-1} and 2885 cm^{-1}), characteristic of C-H stretching vibrations, which belong to the backbone of the different amino acids that constitute *β*-gal. The bands located within the 1700-1500 cm^{-1} range were assigned to the overlap of C=O stretching and N-H bending vibrations, representative of Amide I and Amide II bands, respectively. This band assignment was previously discussed by Baranska et al [35]. Furthermore, *β*-gal displays bands in the 1470-1250 cm^{-1} range corresponding to C-H bending vibrations [35-36]. The Table 2 summarizes the main Raman bands of the non-porous silica support (NPS), the meso-macroporous silica support (MMS) and *β*-gal enzyme with their assignment to the respective characteristic molecular vibrations [35-38].

Table 2. Main Raman bands from the collected spectra (NPS, MMS and free *β*-gal enzyme) and their assignment with the fundamental vibrations, according to the literature [35-38]. (str: stretching, bend: bending, as: asymmetric, s: symmetric).

Sample	**Raman Shift (cm^{-1})**	**Molecular vibration**
NPS	2970	str(as) CH_3
	2908	str CH_2
	2860	str(s) CH_3
	1447	bend C-H
	1310	bend C-H
MMS	2932	str(as) CH_3
	2896	str CH_2
	2855	str(s) CH_3
	1443	bend C-H
	1305	bend C-H
β-gal enzyme	3063	str N-H (Amide B)
	2935	str C-H
	2885	str C-H
	1672	str C=O (Amide I)
	1552	str C-N and bend N-H (Amide II)
	1470-1250	bend C-H

With regards to the spectrum of the MMS materials after *β*-gal immobilization (loaded at the maximum concentration, C), the appearance of the bands corresponding to Amide I, Amide II and Amide B proved the presence of the enzyme on the silica support (Figure 2). It should be

noted that Amide I band suffered a slight displacement to 1666 cm^{-1} when comparing with the free enzyme (1672 cm^{-1}) (Raman uncertainty ±2 cm^{-1}). These amide bands were also observed in the non-porous silica support after *β*-gal immobilization, though they did not display any shift and they were relatively less intense than for the porous silica reacting with the same *β*-gal feed solution. The intensity of the amide bands is reasonably smaller since the amount of adsorbed enzyme is much lower (two orders of magnitude) for the NPS support, at the same enzyme feed solution, C (Table 1).

For better understanding and clearer visualization of the Raman bands of *β*-gal in the MMS/NPS supports after *β*-gal immobilization, the background provided by each support was subtracted (Figure 3). This way, the characteristic Raman bands of *β*-gal are clearly recognizable in both supports (not only amide I band at 1671 cm^{-1}, but also the C-H stretching bands located within 3000-2850 cm^{-1}, which were previously overlapped in Figure 2 by C-H bands of the supports). Furthermore, after subtracting the background support, it can be also noticed in Figure 3 that the amount of adsorbed enzyme on MMS support is larger than the amount adsorbed on NPS support (even though the same enzyme concentration was added to both supports). As described above, this result evidences the higher adsorption of *β*-gal on MMS in comparison to NPS.

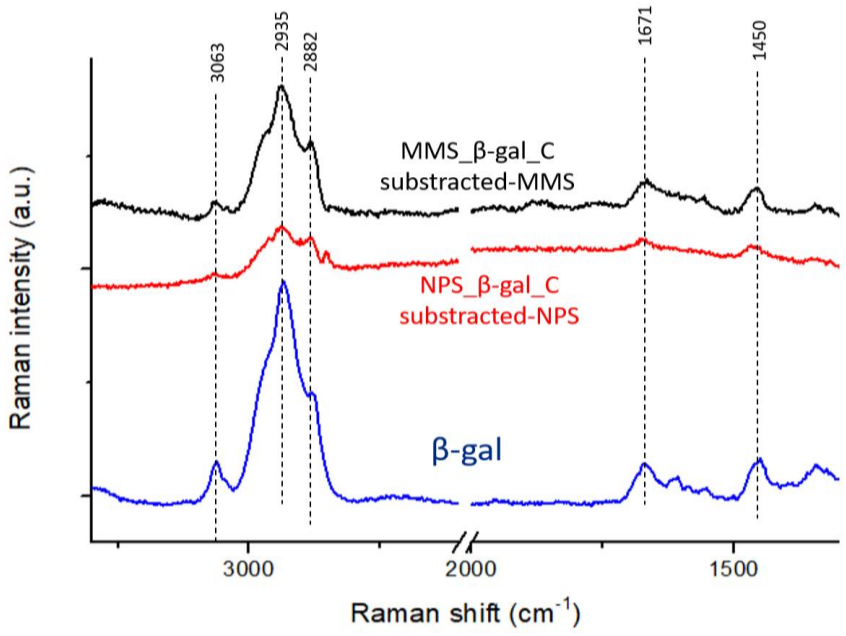

Figure 3: Raman subtracted spectra of NPS and MMS after *β*-gal immobilization. Upper spectrum is the result of subtracting MMS spectrum to MMS- *β*-gal spectrum (of Figure 2). Second spectrum is the result

of subtracting NPS spectrum to NPS- β-gal spectrum (of Figure 2). Raman spectra of lyophilized β-gal free enzyme is also provided for comparison purposes.

In order to examine the strength of the β-gal-silica interactions, additional washings were performed for both silica supports after enzyme immobilization as previously explained in the experimental section. In the case of the β-gal adsorbed on the porous silica support, the supernatant of the first additional washing did not show the presence of protein. On the contrary, for the non-porous silica samples, the supernatant of each additional washing (up to a total of fifteen) still contained released protein, as determined by UV absorption as previously described. This fact supports the outcome that β-gal poorly interacts with the non-porous silica support in contrast to the porous silica support.

Therefore, it appears clearly that the pores are favouring the interactions between the enzyme and the meso-macroporous silica by physical interactions (Van der Walls, hydrophobic and/or electrostatic interaction) leading thus to the entrapment of β-gal. The β-gal presents an isoelectric point of 5.1 while silica has a pI of 2-3. The immobilization process was performed at pH 6.6 to ensure the enzyme stability. At that pH, both the enzyme and the silica support are negatively charged. Previously, it was reported that there is a selective adsorption in the meso-macroporous, arising from the oligomeric complexation of the enzyme (monomer/dimer/tetramer) [18]. As previously explained, monomers or dimers (whose size < 9 nm) can go into the mesopores (ca. 9 nm size), while the tetramers (ca. 14 nm) can be only physisorbed onto the macropores.

The dimers interfaces involve a large number of accessible positively charged residues [18] that, in the presence of negatively charged silanol groups, favour electrostatic enzyme-silica interactions into the mesopores. In addition, the profile of Raman spectrum of MMS_β-gal_C, with respect to the bare material (MMS) spectrum, changes notably in the 3000-2840 cm^{-1} range; there is a change in the intensity ratio of the characteristic str(as) CH_3/str(s) CH_3 bands (see Fig. 2 and Table 2). As this fact does not occur for the adsorption of the enzyme on the NPS, which also contains organic residues, then, the hydrophobic interactions between the

organic residues of the silica materials and the significant proportion of hydrophobic-type interfaces of the dimers [18] must be due to the confinement into the pores.

Then, the sensibility of Raman spectroscopy was inspected for this meso-macroporous support by studying different concentrations of adsorbed *β*-gal. These spectra are shown in Figure 4 A.

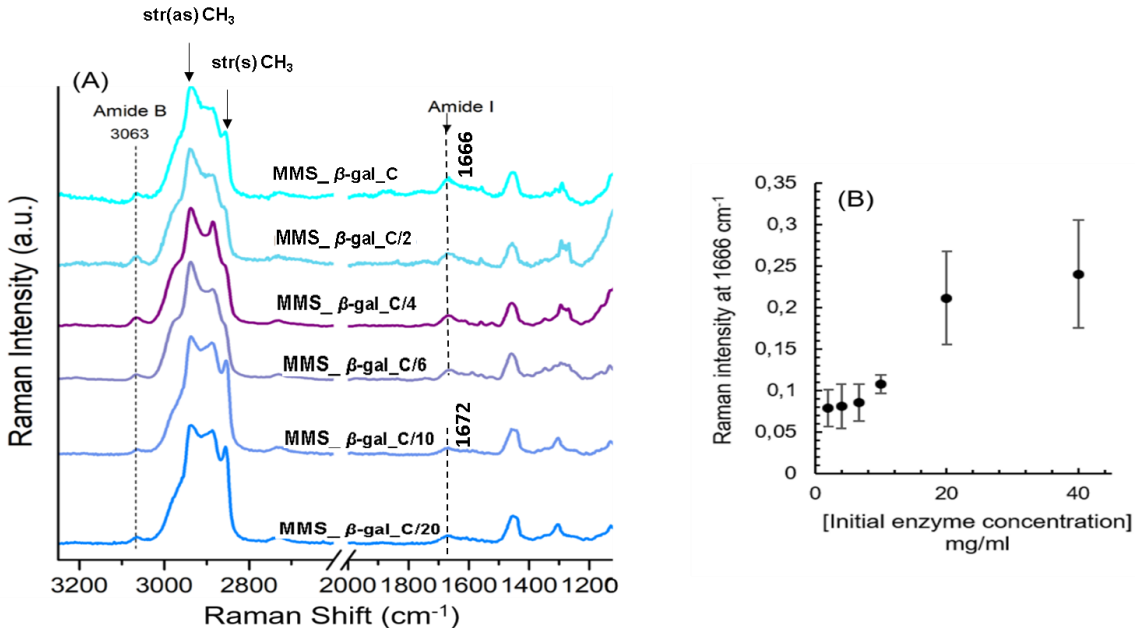

Figure 4. (A) Raman spectra of meso-macroporous (MMS) silica support after *β*-gal immobilization, for different feed solutions at C, C/2, C/4, C/6, C/10 and C/20 (corresponding adsorbed enzyme is given in Table 1); **(B)** Raman intensity at 1666 cm^{-1} as a function of the enzyme concentration in the feed solution (denoted as initial enzyme concentration). The same trend is followed as a function of the adsorbed enzyme.

The increase of the adsorbed enzyme amount may be followed by the intensity's increment of the bands located at 1666 cm^{-1} and 3063 cm^{-1}, assigned to Amide I and Amide B, respectively. In addition, the variation of enzyme concentrations led to a change in the relative intensity of the bands between 2770-3000 cm^{-1} due to the respective C-H vibrations of the enzyme and the support. For the samples containing high enzyme concentrations (C, C/2 and C/4), the band due to the contribution of C-H stretching vibrations from the backbone of the amino acids of *β*-gal (2935 cm^{-1}) was the most intense. However, for the samples containing low enzyme concentrations (C/10 and C/20), the C-H stretching vibrations from the porous silica support (2896 and 2855 cm^{-1}) were dominant over the band from *β*-gal. The spectra also exhibited a slight decrease in the relative intensity of the Amide B band for lower enzyme concentrations.

Although the change in the spectra profiles could be attributed to the progressively increase of enzyme content, there is not a linear effect with the loading degree of the enzyme. Particularly, as displayed in Figure 4 B, the Raman intensity of Amide I band increased with the enzyme concentration of the feed solution, following a sigmoidal function. The inflection point seems to be located around 15 mg/mL of enzyme feed solution. The same trend is followed as a function of the adsorbed *β*-gal (in mg/m^2 MMS). This result is in concordance to our previous study [18], where the physisorption mechanism of the enzyme into the meso-macroporous silica materials depended on the concentration of the enzyme feed solution and on the pore size of the support. In fact, at low initial concentration in enzyme (MMS_*β*-gal_C/20 and MMS_*β*-gal_C/10), no shifts of the amides were recorded on Raman spectra as compared with free enzyme (at 1672 cm^{-1}), indicating a preferential physisorption into macropores. By increasing the enzyme concentration, the frequency of Amide I was shifted to lower values (at 1666 cm^{-1}), suggesting thus a confinement into mesopores. The selective physisorption into the mesoporous may arise from the electrostatic interaction of dimer and silanol groups, compared to the tetramer complexation at higher concentrated feed solutions that guides to a preferred adsorption of the enzyme onto the macropores. Higher enzymes concentrations lead to the aggregation of enzymes that block the diffusion of the enzyme dimers in mesopores [18]. The lower uploading rate, observed at high concentration of enzymes according to TGA or ATR-FTIR analysis [18], results in the *plateau* attained for the Raman intensity (Fig 3B). It should be mention that laser reach enzyme into the mesopores, since the silica wall thickness is lower than 6 nm [18]; i.e., concentration of the enzyme affect similarly the Raman intensity if the enzyme is located into pores or onto external MMS surface. Consequently, both of the red shift of the characteristic amide bands of *β*-gal physisorbed into mesopores vs free enzyme, and the sigmoidal increase of intensity as a function of loading degree, highlight the impact of interactions beyond just an enzyme concentration effect and the confinement of *β*-gal into the meso-macoporous silica.

IR spectroscopy was used in this study as a complementary technique to Raman spectroscopy. Figure 5 displays different IR spectra for an increment of enzyme concentration during the immobilization process for the porous and the non-porous support material.

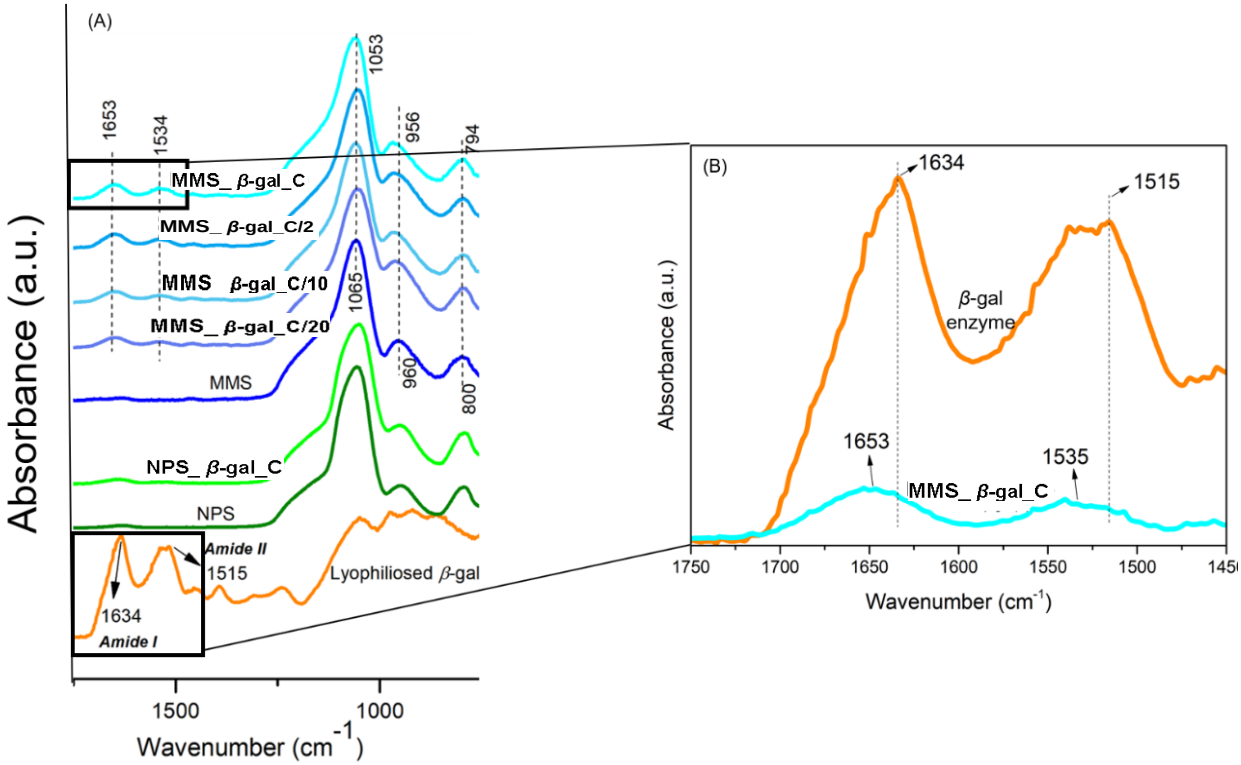

Figure 5. (A) ATR-FTIR spectra of *β*-gal free enzyme, porous (MMS) and non-porous (NPS) silica support before and after *β*-gal immobilization, for different enzyme concentrations (C, C/2, C/10 and C/20 (C=40 mg/ml) for *β*-gal on PS and C for *β*-gal on NPS). (B) Displacement bands of *β*-gal free enzyme in comparison with *β*-gal immobilization on the porous silica (NPS).

Figure 5 clearly shows that the intensity of the amide bands is increasing with the immobilisation rate. As described for the Raman experiments, comparing at the same enzyme feed solution (C, C/2, C/10 and C/20), the intensity of the Amide band I is higher for *β*-gal adsorbed on porous silica (MMS) than on non-porous silica (NPS) samples. The fact is also in agreement with the lower enzyme adsorption onto the NPS particles compared to the MMS material (see Table 1). Regarding samples of *β*-gal adsorbed on meso-macroporous silica, the band assigned to Si-O-Si stretching vibration at 1065 cm^{-1} in the spectrum of the bare porous silica, shifted to 1053 cm^{-1} after *β*-gal immobilization. The band at 960 cm^{-1} assigned to the Si-OH bending vibration, was also displaced to 956 cm^{-1}. Another band at 800 cm^{-1} assigned to Si-O-C stretching vibrations suffered a displacement to 794 cm^{-1} after enzyme adsorption on the porous support. All those vibrations that involved the silica material have lower energy, and the chemical bonds are certainly less interacting with the enzyme.

Moreover, the centre of the maxima of the Amide I and Amide II bands of the free β-gal enzyme shift from 1634 cm^{-1} to 1653 cm^{-1} and 1515 cm^{-1} to 1535 cm^{-1}, respectively, for the enzyme-silica samples (see inset Fig. 4). The amide I is sensitive to particular secondary structural conformation and consists of many overlapping component bands that represents different structures: purely α-helices, β-sheets, turns and unordered or irregular structures. The maximum band at 1634 cm^{-1} corresponds to β-sheet structures, while 1653 cm^{-1} is associated to a more random coil contribution [39]. As the wavelength range of the broad band's contour doesn't change after the adsorption of the enzyme, the shift of the maxima are related to the change of integrated intensities areas of its individual underlying band subcomponents, i.e., conformational changes of the adsorbed enzyme.

Remarkably, no spectral shifts or broadening were observed neither for the enzyme bands adsorbed on the non-porous material nor for the silica material vibrations. This result demonstrates again the weaker interaction in the loaded β-gal enzyme onto the non-porous support in comparison to the porous meso-macroporous support as previously evidenced by Raman. Thus, the porosity seems to be the key factor in the enzyme entrapment and thus adsorption.

4. Conclusions

In this study, the capability of Raman spectroscopy to prove the adsorption of β-gal on meso-macroporous silica support was demonstrated by the shifts occurring for the amide bands of the β-gal spectra. In addition, a different profile of Raman spectrum of MMS_β-gal_C sample with respect to the bare material (MMS) spectrum, in the 3000-2840 cm^{-1} range, was observed. For that reason, it is expected that the amide groups are mainly involved in the interaction that occurred between the enzyme and silica, but also in the hydrophobic forces between the organic

residues of the silica material and the aminoacid backbone of the enzyme, probably favoured by the enzyme confinement into the porous.

Thus, the morphology of the silica material seems to be the key factor in the enzyme adsorption. The physically enzyme adsorption is strongly favoured by the enzyme entrapment into the pores. While the *β*-gal physisorbed on the surface of non-porous silica material exhibits the same Raman spectra as the free enzyme, the enzyme physisorbed onto meso-macroporous materials show frequency displacements of characteristic amide groups as a function of initial concentration of the feed enzymatic solution. In fact, at low initial concentration in enzyme, no shifts of the amides were recorded on Raman spectra as compared with free enzyme, indicating a preferential physisorption into macropores. In addition, almost all *β*-gal was released in the supernatant recovered from the non-porous samples during washing steps, contrary to the porous samples. All these facts together evidence a stronger interaction between *β*-gal and the meso-macroporous silica support than with the NPS material.

Finally, it was observed that the intensity of the Raman amide bands bears a sigmoidal increment by increasing the content of the adsorbed enzyme. The enzyme complexation was determined in our previous theoretical studies [18]. Further, chemometric analysis could help to inspect the variability of samples with different amount of adsorbed *β*-gal on different silica supports by vibrational spectroscopy.

Acknowledgments

The research leading to these results has received funding from the People Programme (Marie Curie Actions) of the European Union's Seventh Framework Programme FP7/2007-2013/ under REA grant agreement n° 606713 – BIBAFOODS. The authors want to acknowledge CHR-HANSEN Company for providing the enzyme solution and NPS material. Finally, authors would like to acknowledge the valuable scientific discussion about spectroscopy provided by Rafael Sánchez; the experimental support provided by Diogo Videira-Quintela with SEM

images and enzyme adsorption on NPS particles; and the experimental support provided by Alba Blánquez Moya with the lyophilisation of samples.

References

[1] M. Komiyama, K. Yoshimoto, M. Sisido, K. Ariga, Chemistry Can Make Strict and Fuzzy Controls for Bio-Systems: DNA Nanoarchitectonics and Cell-Macromolecular Nanoarchitectonics. *Bull. Chem. Soc. Jpn.* 90 (2017) 967-1004.

[2] X. Xiao, P. Conghaile, D. Leech, R. Ludwig, E. Magne, A symmetric supercapacitor/biofuel cell hybrid device based on enzyme-modified nanoporous gold: An autonomous pulse generator. *Biosens. Bioelectron.* 90 (2017) 96-102.

[3] C. Doonan, R. Ricco, K. Liang, D. Bradshaw, P. Falcaro. Metal–Organic Frameworks at the Biointerface: Synthetic Strategies and Applications. *Acc. Chem. Res.* 50 (2017) 1423-1432.

[4] L. Yuxuan, W. Lijun, L. Yuan, Y. Gaojian, T. Congli, D. Yan, L. Song. Immunosensors Based on Nanomaterials for Detection of Tumor Markers. *J. Biomed. Nanotechnol.* 14 (2018) 44-65.

[5] J. Zdarta, A. Meyer, T. Jesionowski, M. Pinelo. A General Overview of Support Materials for Enzyme Immobilization: Characteristics, Properties, Practical Utility. *Catalysts* 8 (2018) 92.

[6] A. Bernardos, E. Aznar, M. Marcos, F. Sancenón, J. Soto, J. Barat, P. Amorós. Enzyme- Responsive Controlled Release Using Mesoporous Silica Supports Capped with Lactose. *Angew. Chem. Int.* Ed. 48 (2009) 5884 –5887.

[7] A. Bernardos, L. Mondragón, E. Aznar, M. Marcos, R. Martínez-Máñez, F. Sancenón, J. Soto, J. Barat, E. Pérez-Pavá, C. Guillem, P. Amorós. Enzyme-Responsive Intracellular Controlled Release Using Nanometric Silica Mesoporous Supports Capped with "Saccharides". *ACS Nano* 4 (11), (2010) 6353–6368.

[8] J. Chao, H. Liu, S. Su, L. Wang, W. Huang, C. Fan. Structural DNA Nanotechnology for Intelligent Drug Delivery. *Small* 10 (22) (2014) 4626-4635.

[9] V. Linko, A. Ora, M. Kostiainen. DNA Nanostructures as Smart Drug-Delivery Vehicles and Molecular Devices. Trends Biotechnol. 33 (2015), 586-594.

[10] T. Jesionowski, J. Zdarta, B. Krajewska, Enzyme immobilization by adsorption: a review. *Adsorption* 20 (2014) 801-821.

[11] F. Contesini, J. de Alencar Figueira, H. Kawaguti, P. de Barros Fernandes, P. de Oliveira Carvalho, M. da Graça Nascimento, H. Sato, Potential Applications of Carbohydrases Immobilization in the Food Industry, *Int. J. Mol. Sci.* 14 (2013) 1335-1369.

[12] Braga, A.R.C., Silva, M.F., Oliveira, J.V., Treichel, H., and Kalil, S.J., A new approach to evaluate immobilization of *β*-galactosidase on Eupergit® C: structural, kinetic, and thermal characterization. Quim. Nova, 37 (2014) 796–803.

[13] Nath, A., Mondal, S., Chakraborty, S., Bhattacharjee, C., and Chowdhury, R., Production, purification, characterization, immobilization, and application of b-galactosidase: a review. Asia-Pacific J. Chem. Eng., 9 (2014) 330–348.

[14] C. Bernal, L. Sierra, M. Mesa, Application of hierarchical porous silica with a stable large porosity for *β*-galactosidase immobilization, *Chem. Cat. Chem.* 3 (2011) 1948-1954.

[15] C. Bernal, L. Sierra, M. Mesa, Improvement of Thermal Stability of *β*-Galactosidase from Bacillus Circulans by Multipoint Covalent Immobilization in Hierarchical Macro-Mesoporous Silica, *J. Mol. Catal. B: Enzym.* 84 (2012) 166-172.

[16] C. Bernal, P. Urrutia, A. Illanes, L. Wilson, Hierarchical meso-macroporous silica grafted with glyoxyl groups: opportunities for covalent immobilization of enzymes, *New Biotechnol.* 30 (2013) 500-506.

[17] A. K. Meka, P. L. Abbaraju, H. Song, C. Xu, J. Zhang, H. Zhang, M. Yu, C. Yu, A vehicle supra-assembly approach to synthesize amine-functionalized hollow dendritic mesoporous silica nanospheres for protein delivery, *Small* 12(37) (2016) 5169-5177.

[18] S. F. Prazeres. I. A. Pavel, G. Montalvo, C. Garcia-Ruiz, V. Nicolas, A. Celzard, F. Dehez, L. Canabady-Rochelle, N. Canilho, A. Pasc, Effect of meso vs macro-size of hierarchical porous silica on the adsorption and activity of immobilized *β*-galactosidase, *Langmuir* 33 (2017) 3333-3340.

[19] I. Pavel, M. Girardon, S. El Hajj, S. Parant, F. Amadei, S. Kaufmann, M. Tanaka, V. Fierro, A. Celzard, N. Canilho, A. Pasc, Lipid-coated mesoporous silica microparticles for controlled delivery of *β*-galactosidase into intestine, *J. Mater. Chem. B* 6 (2018) 5633-5639.

[20] I. González-Delgado, Y. Segura, A. Martín, M. López-Muñoz, G. Morales, *β*-galactosidase covalent immobilization over large-pore mesoporous silica supports for the production of high galacto-oligosaccharides (GOS), *Microporous Mesoporous Mater.* 257 (2018) 51-61.

[21] P. Larkin, Infrared and Raman spectroscopy principles and spectral interpretation; Elsevier: Amsterdam, The Netherlands, 2011.

[22] S. F. Prazeres, C. García-Ruiz, G. Montalvo, Vibrational Spectroscopy as a Promising Tool to Study Enzyme-Carrier Interactions: A Review, *Appl. Spectrosc.* 50 (2015) 797-821.

[23] R. Reshmi, G. Sanjay, S. Sugunan, Enhanced activity and stability of α-amylase immobilized on alumina. *Catal. Commun.* 7 (2006) 460-465.

[24] M. L. Verma, C. J. Barrow, J. F. Kennedy, M. Puri, Immobilization of *β*-d-galactosidase from Kluyveromyces lactis on functionalized silicon dioxide nanoparticles: Characterization and lactose hydrolysis, *Int. J. Biol. Macromol.* 50 (2012) 432-437.

[25] S. Wang, P. Su, F. Ding, Y. Yang, Immobilization of cellulase on polyamidoamine dendrimer-grafted silica, *J. Mol. Catal. B: Enzym.* 89 (2013) 35-40.

[26] K. K. Chittur, FTIR/ATR for protein adsorption to biomaterial surfaces, *Biomaterials* 19 (1998) 357-369.

[27] K. P. Dhake, A. H. Karoyo, M. H. Mohamed, L. D. Wilson, B. M. Bhanage, Enzymatic activity studies of Pseudomonas cepacia lipase adsorbed onto copolymer supports containing *β*-cyclodextrin, *J. Mol. Catal. B: Enzym.* 87 (2013) 105-112.

[28] M. Falahati, L. Ma'mani, A. A. Saboury, A. Shafiee, A. Foroumadi, A. R. Badiei, Aminopropyl-functionalized cubic Ia3d mesoporous silica nanoparticle as an efficient support for immobilization of superoxide dismutase, *Biochim. Biophys. Acta* 1814 (2011) 1195-1202.

[29] V. Patel, H. Gajera, A. Gupta, L. Manocha, D. Madamwar, Synthesis of ethyl caprylate in organic media using Candida rugosa lipase immobilized on exfoliated graphene oxide: Process parameters and reusability studies, *Biochem. Eng. J.* 95 (2015) 62-70.

[30] P. Hildebrandt, M. Stockburger, Cytochrome C at charged interfaces. 1. Conformational and redox equilibria at the electrode/electrolyte interface probed by surface-enhanced resonance Raman spectroscopy, *Biochemistry* 28 (1989) 6710-6721.

[31] Y. Chen, S. Han, X. Li, Z. Zhang, S. Ma, Why Does Enzyme Not Leach from Metal–Organic Frameworks (MOFs)? Unveiling the Interactions between an Enzyme Molecule and a MOF, *Inorg. Chem.* 53 (2014) 10006-10008.

[32] R. Ravetti-Duran, J. L. Blin, M. J. Stebe, C. Castel, A. Pasc, Tuning the morphology and the structure of hierarchical meso-macroporous silica by dual templating with micelles and solid lipid nanoparticles (SLN), *J. Mater. Chem.* 22 (2012) 21540-21548.

[33] A. J. Engelen, P. H. Randsdorp, Determination of neutral lactase activity in industrial enzyme preparations by a colorimetric enzymatic method: collaborative study, *J AOAC Int* 82 (1999) 112-118.

547 [34] A. S. Poyraz, C. Albayrak, Ö. Dag, The effect of cationic surfactant and some
548 organic/inorganic additives on the morphology of mesostructured silica templated by pluronics,
549 *Microporous Mesoporous Mater.* 115 (2008) 548-555.

550 [35] A. Rygula, K. Majzner, K. M. Marzec, A. Kaczor, M. Pilarczyk, M. Baranska, Raman
551 spectroscopy of proteins: a review, *J. Raman Spectrosc.* 44 (2013) 1061-1076.

552 [36] K. S. Singh, M. S. Majik, S. Tilvi, Vibrational Spectroscopy for Structural Characterization
553 of Bioactive Compounds, Analysis of Marine Samples in Searche of Bioactive Compounds,
554 Elsevier (Ed.), 65 (2014) 115-141.

555 [37] P. J. Launer (updated by Arkles), Infrared analysis of organosilicon compounds: spectra-
556 structure correlations, Silicon Compounds Register and Review (4^{th} edition S-7), Ed. R.
557 Anderson, B. Arkles, G. Larson, Petrarch Systems, Inc. Bristol, PA, (1987) 100-103.

558 [38] M. Badertscher, P. Bühlmann, E. Pretsch, Structure Determination of Organic Compounds,
559 Springer, Berlin Heidelberg, (2009).

560 [39] A. Dong, P. Huang, W. S. Caughey, Protein Secondary Structures in Water from 2^{nd}-
561 Derivative Amide-I Infrared-Spectra. *Biochemistry* 29 (1990) 3303-3308.

562

Figure 1

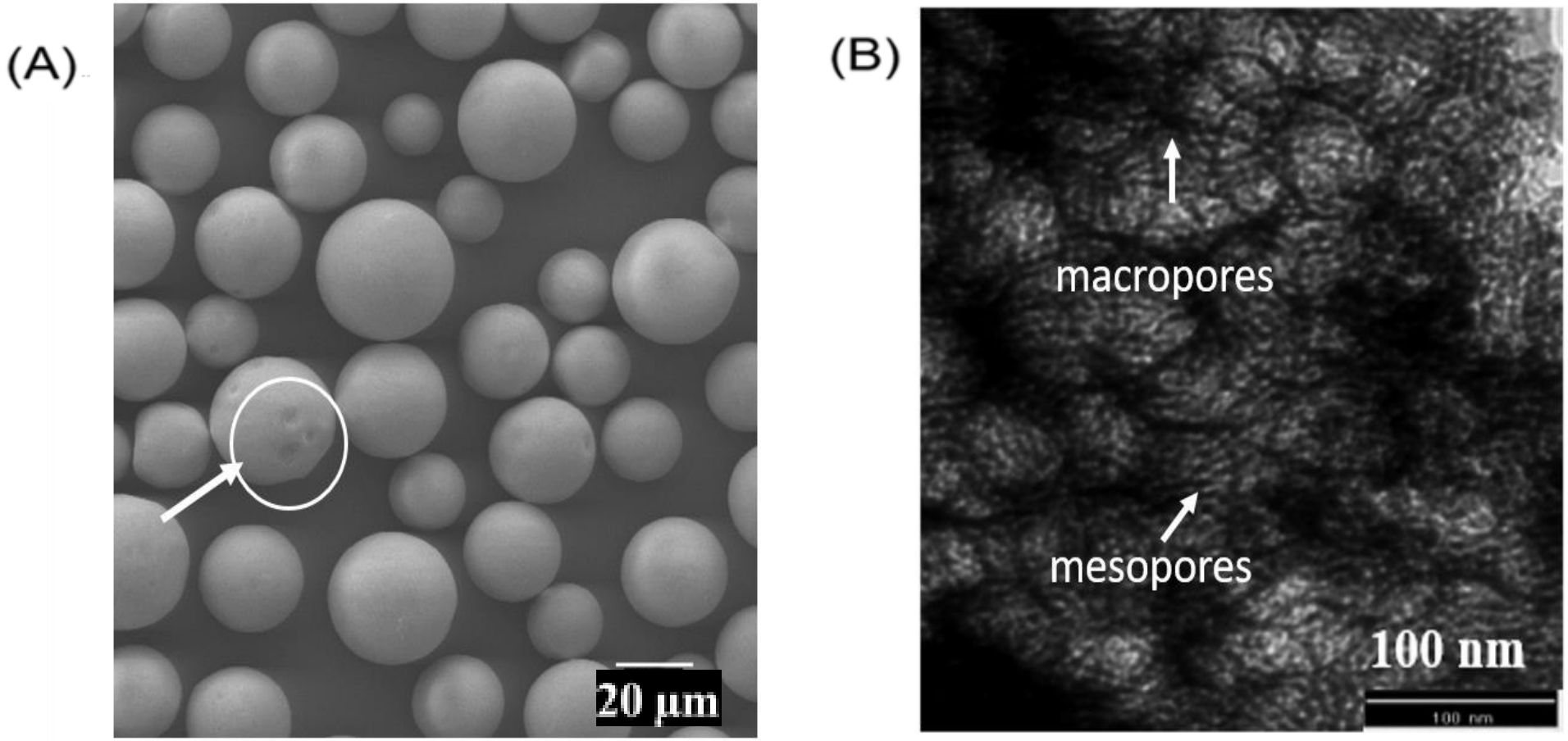

FIGURE 1

Figure 2

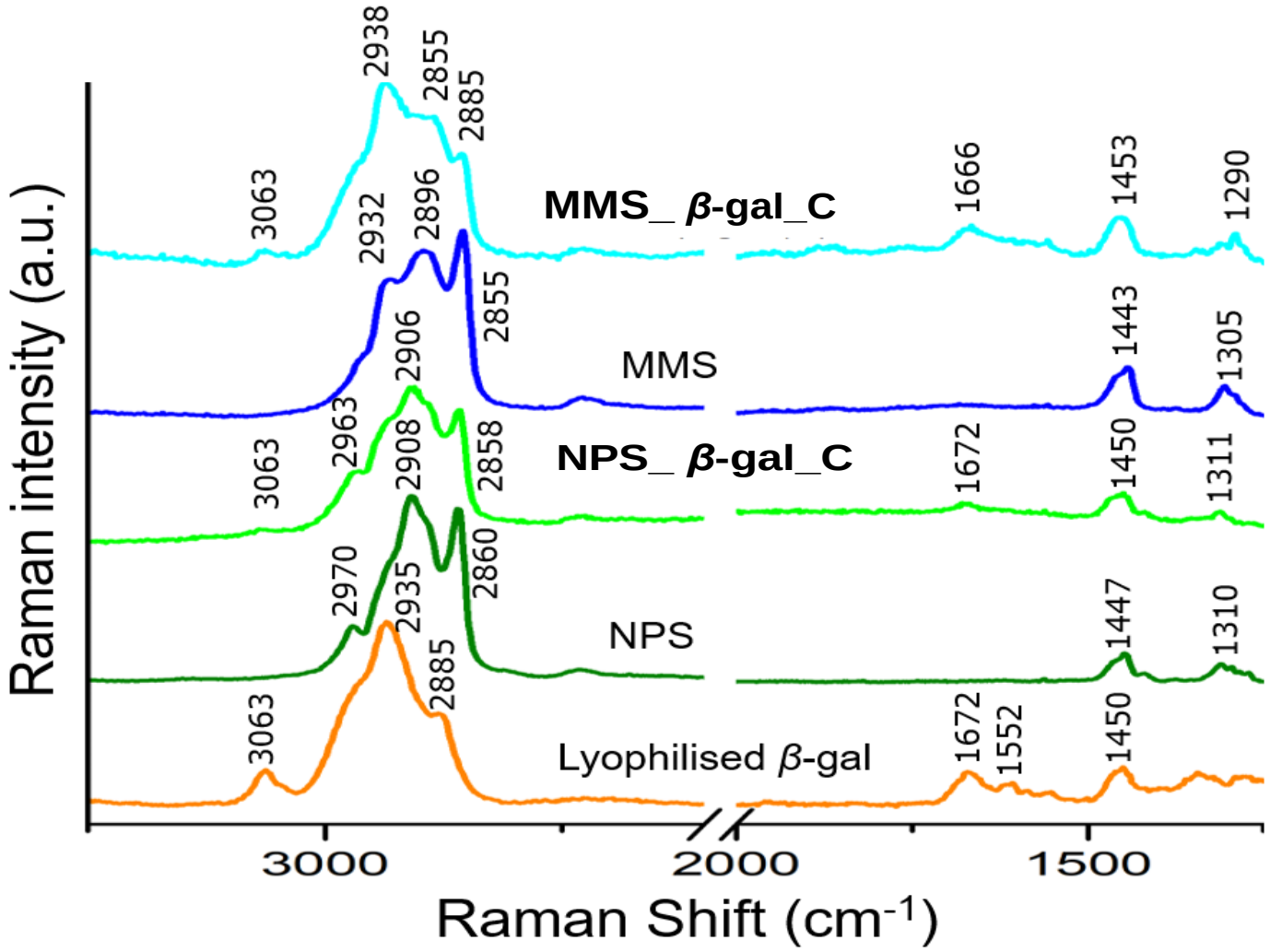

FIGURE 2

Figure 3

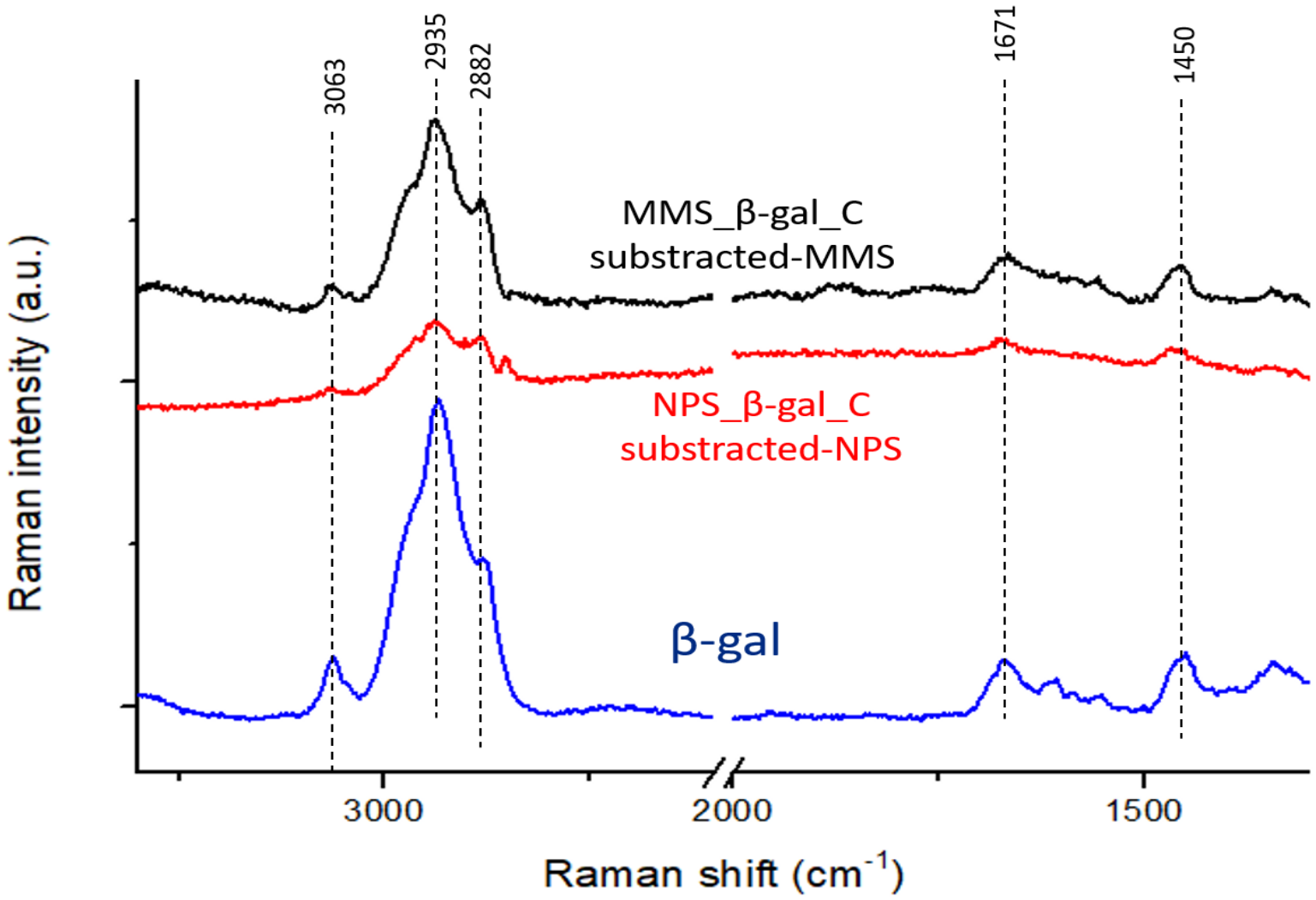

FIGURE 3

Figure 4

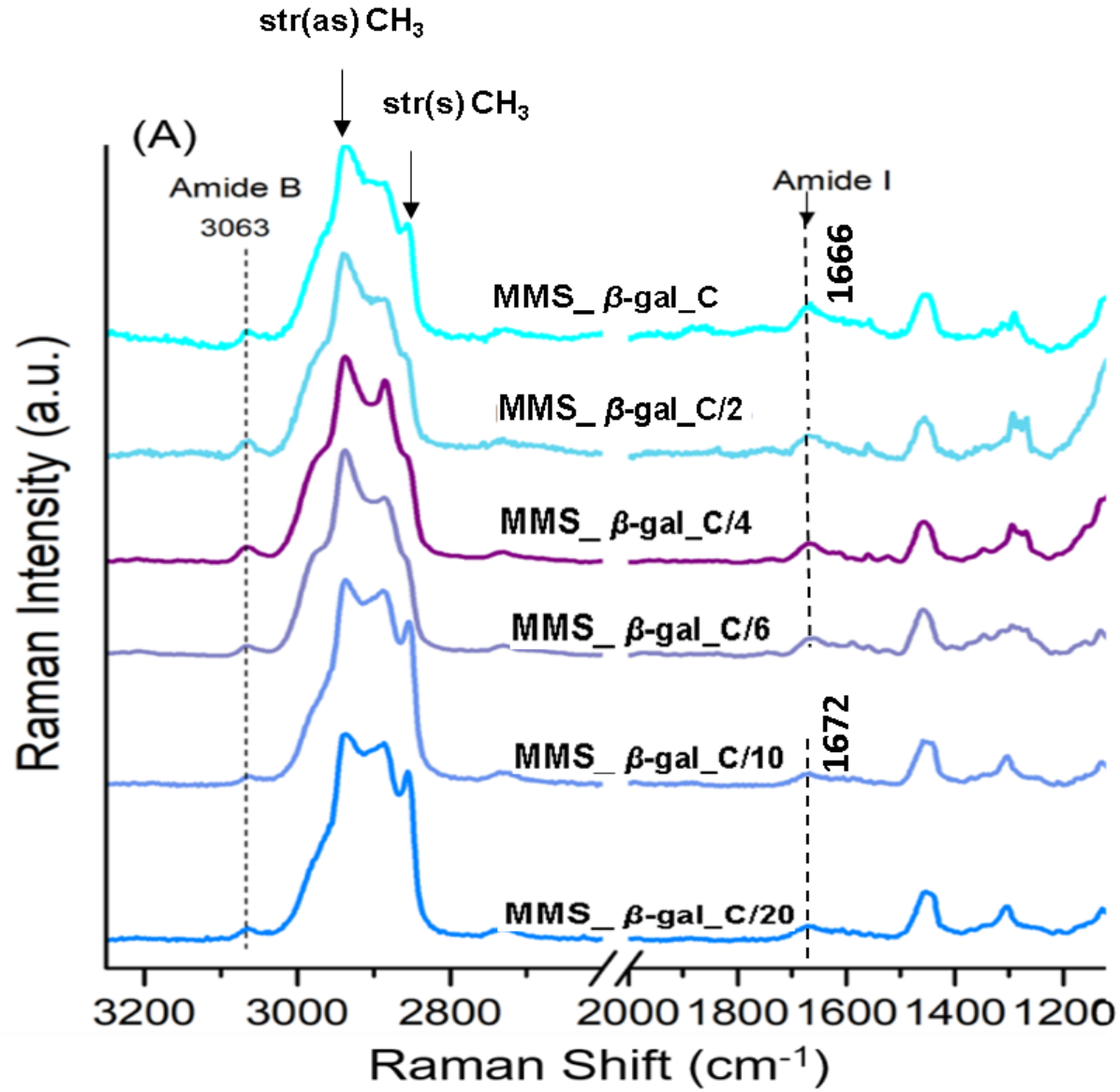

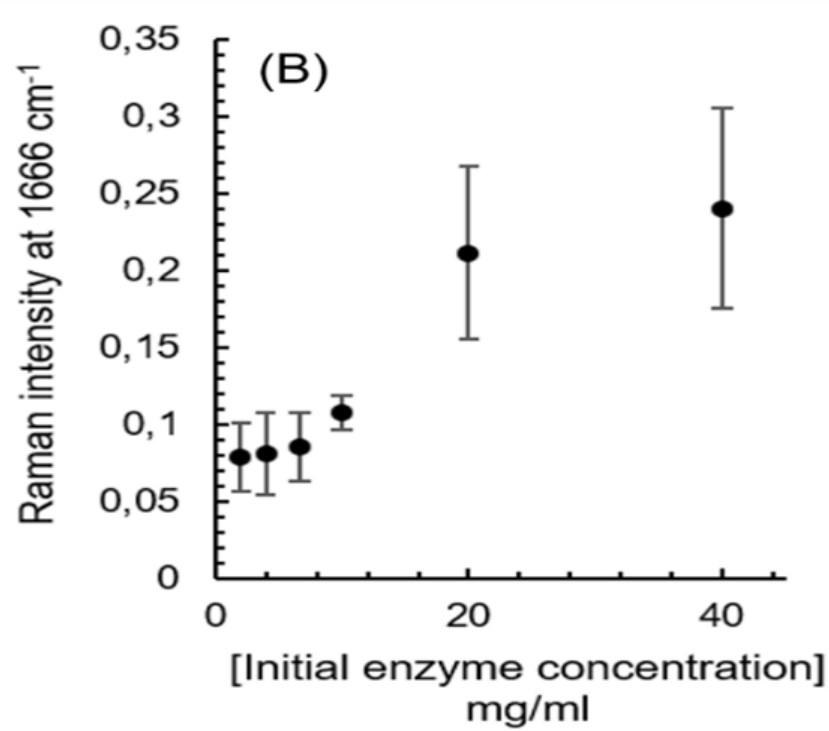

FIGURE 4

Figure 5

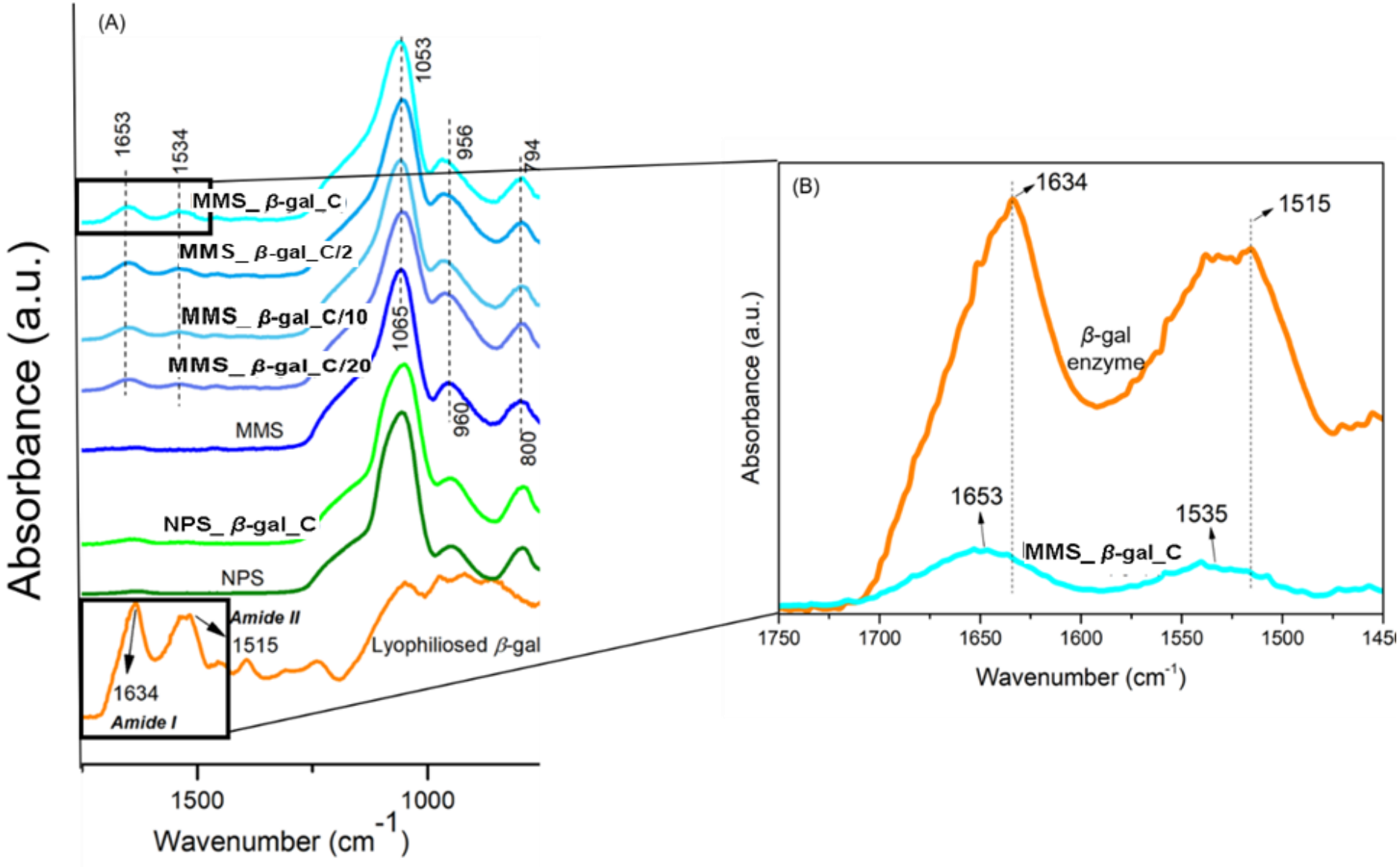

FIGURE 5

Table 1. Amount of *β*-gal adsorbed on MMS per surface area of MMS, for the different concentrations of initial β-gal solutions used for immobilization.

Sample	Initial *β*-gal concentration (mg/mL)	Adsorbed *β*-gal (mg/ m^2)
MMS_*β*-gal_C	40	16
MMS_*β*-gal_C /2	20	10
MMS_*β*-gal_C /4	10	8.0
MMS_*β*-gal_C /6	6.7	6.9
MMS_*β*-gal_C /10	4.0	5.2
MMS_*β*-gal_C C/20	2.0	5.2

Probing the confinement of *β*-galactosidase into meso-macro porous silica by Raman spectroscopy

Sofia F. Prazeres[1], Félix Zapata[1,2], Nadia Canilho[3], Andreea Pasc[3], Carmen García-Ruiz[1, 2]; Gemma Montalvo[1, 2,*]

[1]Department of Analytical Chemistry, Physical Chemistry and Chemical Engineering, University of Alcalá, Ctra. Madrid-Barcelona Km. 33.600, 28871 Alcalá de Henares, Madrid, Spain

[2]University Institute of Research in Police Sciences, University of Alcalá, Ctra. Madrid-Barcelona Km. 33.600, 28871 Alcalá de Henares, Madrid, Spain

[3]L2CM UMR 7053 CNRS-Universite de Lorraine, Bvd des Aiguillettes, BP 70239, F-54506 Vandoeuvre-les-Nancy, France

* Corresponding author: gemma.montalvo@uah.es

Table 2. Main Raman bands from the collected spectra (NPS, MMS and free *β*-gal enzyme) and their assignment with the fundamental vibrations, according to the literature [17-21]. (str: stretching, bend: bending, as: asymmetric, s: symmetric).

Sample	Raman Shift (cm^{-1})	Molecular vibration
NPS	2970	str(as) CH_3
	2908	str CH_2
	2860	str(s) CH_3
	1447	bend C-H
	1310	bend C-H
MMS	2932	str(as) CH_3
	2896	str CH_2
	2855	str(s) CH_3
	1443	bend C-H
	1305	bend C-H
β-gal enzyme	3063	str N-H (Amide B)
	2935	str C-H
	2885	str C-H
	1672	str C=O (Amide I)
	1552	str C-N and bend N-H (Amide II)
	1470-1250	bend C-H

Probing the confinement of *β*-galactosidase into meso-macro porous silica by Raman spectroscopy

Sofia F. Prazeres[1], Félix Zapata[1,2], Nadia Canilho[3], Andreea Pasc[3], Carmen García-Ruiz[1, 2]; Gemma Montalvo[1, 2,*]

[1]Department of Analytical Chemistry, Physical Chemistry and Chemical Engineering, University of Alcalá, Ctra. Madrid-Barcelona Km. 33.600, 28871 Alcalá de Henares, Madrid, Spain

[2]University Institute of Research in Police Sciences, University of Alcalá, Ctra. Madrid-Barcelona Km. 33.600, 28871 Alcalá de Henares, Madrid, Spain

[3]L2CM UMR 7053 CNRS-Universite de Lorraine, Bvd des Aiguillettes, BP 70239, F-54506 Vandoeuvre-les-Nancy, France

* Corresponding author: gemma.montalvo@uah.es